Available online at www.sciencedirect.com

ScienceDirect

Nuclear Physics A 982 (2019) 531–534

NUCLEAR PHYSICS A

www.elsevier.com/locate/nuclphysa

XXVIIth International Conference on Ultrarelativistic Nucleus-Nucleus Collisions (Quark Matter 2018)

Re-examining the premise of isobaric collisions and a novel method to measure the chiral magnetic effect

Hao-jie Xu[a], Jie Zhao[b], Xiaobao Wang[a], Hanlin Li[c], Zi-Wei Lin[d,e], Caiwan Shen[a], Fuqiang Wang[a,b]

[a]*School of Science, Huzhou University, Huzhou, Zhejiang 313000, China*
[b]*Department of Physics and Astronomy, Purdue University, West Lafayette, Indiana 47907, USA*
[c]*College of Science, Wuhan University of Science and Technology, Wuhan, Hubei 430065, China*
[d]*Department of Physics, East Carolina University, Greenville, North Carolina 27858, USA*
[e]*Key Laboratory of Quarks and Lepton Physics (MOE) and Institute of Particle Physics, Central China Normal University, Wuhan, Hubei 430079, China*

Abstract

In these proceedings we show that the premise of the isobaric $^{96}_{44}$Ru +$^{96}_{44}$ Ru and $^{96}_{40}$Zr +$^{96}_{40}$ Zr collisions to search for the chiral magnetic effect (CME) may not hold as originally anticipated due to large uncertainties in the isobaric nuclear structures. We demonstrate this using Woods-Saxon densities and the proton and neutron densities calculated by the density functional theory. Furthermore, a novel method is proposed to gauge background and possible CME contributions in the same system, intrinsically better than the isobaric collisions of two different systems. We illustrate the method with Monte Carlo Glauber and AMPT (A Multi-Phase Transport) simulations.

Keywords: chiral magnetic effect, isobaric collisions, density functional theory

1. Introduction

In quantum chromodynamics (QCD), the interactions of quarks with topological gluon fields can induce chirality imbalance and parity violation in local domains under the approximate chiral symmetry restoration [1]. A chirality imbalance could lead to an electric current, or charge separation (CS) in the direction of a strong magnetic field (**B**). This phenomenon is called the chiral magnetic effect (CME) [1]. Searching for the CME is one of the most active research in heavy ion collisions (HIC) [2, 3]. In HIC the CS is commonly measured by the three-point correlator [4], $\gamma \equiv \cos(\phi_\alpha + \phi_\beta - 2\psi_{\rm RP})$, where ϕ_α and ϕ_β are the azimuthal angles of two charged particles, and $\psi_{\rm RP}$ is that of the reaction plane (RP, spanned by the impact parameter and beam directions) to which the **B** produced by the incoming protons is perpendicular on average. Positive $\Delta\gamma \equiv \gamma_{\rm OS} - \gamma_{\rm SS}$ (OS:opposite-sign, SS:same -sign) signals, consistent with the CME-induced CS perpendicular to the RP, have been observed [5]. The signals are, however, inconclusive because of a large charge-dependent background arising from particle correlations (e.g. resonance decays) coupled with the elliptic flow anisotropy (v_2) [6].

https://doi.org/10.1016/j.nuclphysa.2018.11.031

To better control the background, isobaric collisions of $^{96}_{44}$Ru+$^{96}_{44}$Ru (RuRu) and $^{96}_{40}$Zr+$^{96}_{40}$Zr (ZrZr) have been proposed [7]. One expects their backgrounds to be almost equal because of the same mass number, while the atomic numbers, hence **B**, differ by 10%. This is verified by *Monte Carlo* Glauber (MCG) calculations using the Woods-Saxon (WS) density profile [8]. As a net result, the CME signal-to-background ratio would be improved by over a factor of 7 in comparative measurements between RuRu and ZrZr collisions than in each of them individually [8]. The isobaric collisions are planned for 2018 at RHIC; they would yield a CME signal of 5σ significance with the projected data volume, if one assumes that the CME contributes 1/3 of the current $\Delta\gamma$ measurement in AuAu collisions.

However, there can be non-negligible deviations of the Ru and Zr nuclear densities from WS. In these proceedings, we show their effects on the sensitivity of isobaric collisions for the CME search [9], and propose a novel method to avoid those uncertainties [10].

2. Re-examining the premise of isobaric collisions

Because of the different numbers of protons–which suffer from Coulomb repulsion–and neutrons, the structures of the $^{96}_{44}$Ru and $^{96}_{40}$Zr nuclei must not be identical. By using density functional theory (DFT), we calculate the Ru and Zr proton and neutron distributions using the well-known SLy4 mean field including pairing correlations (Hartree-Fock-Bogoliubov, HFB approach) [11]. Those density distributions are shown in Fig. 1. Protons in Zr are more concentrated in the core, while protons in Ru, 10% more than in Zr, are pushed more toward outer regions. The neutrons in Zr, four more than in Ru, are more concentrated in the core but also more populated on the nuclear skin. Theoretical uncertainties are estimated by using different sets of density functionals, SLy5 and SkM* for the mean field, with and without pairing (HFB/HF), and are found to be small.

The ϵ_2 of the transverse overlap geometry in RuRu and ZrZr collisions is calculated event-by-event with MCG [12], using the DFT nucleon densities in Fig. 1. $\mathbf{B}(\mathbf{r}, t = 0)$ is also calculated for RuRu and ZrZr collisions using the DFT proton densities. The calculations follow Ref. [13], with a finite proton radius (0.88 fm is used but the numeric value is not critical) to avoid the singularity at zero relative distance. Two reference planes are used for each collision system: reaction plane ($\psi_{\rm RP}$) and participant plane ($\psi_{\rm PP}$). For the CME search with isobaric collisions, the relative differences in ϵ_2 and $B_{\rm sq}$ are of importance. Figure 2 shows the relative differences $R(\epsilon_2\{\psi_{\rm PP}\})$, $R(\epsilon_2\{\psi_{\rm RP}\})$, $R(B_{\rm sq}\{\psi_{\rm PP}\})$, and $R(B_{\rm sq}\{\psi_{\rm RP}\})$; $R(X)$ is defined as

$$R(X) \equiv 2(X_{\rm RuRu} - X_{\rm ZrZr})/(X_{\rm RuRu} + X_{\rm ZrZr}) \tag{1}$$

where $X_{\rm RuRu}$ and $X_{\rm ZrZr}$ are the X values in RuRu and ZrZr collisions, respectively. The thick solid curves are the default results with the DFT densities in Fig. 1. The shaded areas correspond to theoretical uncertainties bracketed by the two DFT density cases where Ru is deformed with $\beta_2 = 0.158$ and Zr is spherical and where Ru is spherical and Zr is deformed with $\beta_2 = 0.217$. The hatched areas represent our results using WS densities with the above two cases of nuclear deformities.

We also investigate whether our density profiles would, in a dynamical model, lead to a final-state v_2 difference between RuRu and ZrZr collisions and whether the $B_{\rm sq}$ difference preserves with respect to the event plane (EP) reconstructed from the final-state particle momenta. We employ A Multi-Phase Transport (AMPT) model with "string melting" [14], which can reasonably reproduce heavy ion bulk data at RHIC and the LHC. We found that the general trends are similar to those in Fig. 2 [9].

From the MCG and AMPT simulations, we find that the DFT nuclear densities, together with the Woods-Saxon (WS) densities, yield wide ranges of differences in $B_{\rm sq}$ with respect to the participant plane (PP) and the reaction plane (RP). It is further found that those nuclear densities introduce, in contrast to WS, comparable differences in $\epsilon_2\{\psi_{\rm RP}\}$ ($v_2\{\psi_{\rm RP}\}$) and $B_{\rm sq}\{\psi_{\rm RP}\}$ with respect to the reaction plane (RP), diminishing the premise of isobaric collisions to help identify the CME. With respect to the participant plane (PP), the $\epsilon_2\{\psi_{\rm PP}\}$ ($v_2\{\psi_{\rm EP}\}$) difference can still be sizable, as large as $\sim 3\%$, possibly weakening the power of isobaric collisions for the CME search [9]. For example, if only 10% of the measured $\Delta\gamma$ comes from the CME signal, then the B_{sq} difference of 20% would introduce only a 2% effect, while the elliptic flow difference gives a 2.4% effect.

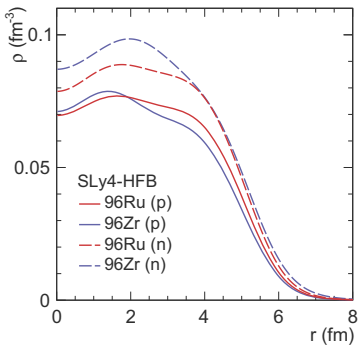

Fig. 1. (Color online) Proton and neutron density distributions of the $^{96}_{44}$Ru and $^{96}_{40}$Zr nuclei, assumed spherical, calculated by the DFT method.

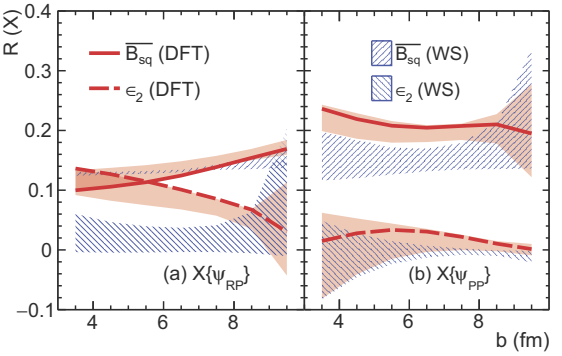

Fig. 2. (Color online) Relative differences between RuRu and ZrZr collisions in $\epsilon_2\{\psi\}$ and $B_{sq}\{\psi\}$ with respect to (a) $\psi = \psi_{RP}$ and (b) $\psi = \psi_{PP}$, using the DFT densities. The shaded areas correspond to DFT density uncertainties from Ru and Zr deformities; the hatched areas show the corresponding results using WS density distributions.

3. A novel method to measure the CME

Based on the above study [9], we found that with respect to ψ_{PP}, v_2 is stronger than that with respect to ψ_{RP}. This is because elliptic flow (v_2) develops in relativistic heavy ion collisions from the anisotropic overlap geometry of the participant nucleons. The magnetic field (**B**) is, on the other hand, produced mainly by spectator protons and its direction fluctuates nominally about ψ_{RP}, not ψ_{PP}. Therefore, **B** with respect to ψ_{PP} is weaker than **B** with respect to ψ_{RP}. Our new method is based on these opposite behaviors in the fluctuations of the magnetic field and v_2 in a single nucleus-nucleus collision, thus bears minimal theoretical and experimental uncertainties. It is convenient to define a relative difference [10],

$$R^{\mathrm{PP(EP)}}(X) \equiv 2 \cdot \frac{X\{\psi_{\mathrm{RP}}\} - X\{\psi_{\mathrm{PP(EP)}}\}}{X\{\psi_{\mathrm{RP}}\} + X\{\psi_{\mathrm{PP(EP)}}\}}\,, \tag{2}$$

where $X\{\psi_{RP}\}$ and $X\{\psi_{PP(EP)}\}$ are the measurements of quantity X with respect to ψ_{RP} and ψ_{PP} (or ψ_{EP} described below), respectively. The upper panels of Fig. 3 show $R^{PP}(\epsilon_2)$ and $R^{PP}(B_{sq})$ calculated by a MCG model for $^{197}_{79}$Au+$^{197}_{79}$Au (AuAu), $^{62}_{29}$Cu+$^{62}_{29}$Cu (CuCu), RuRu, ZrZr collisions at RHIC and $^{207}_{82}$Pb+$^{207}_{82}$Pb (PbPb) collisions at the LHC. Although a theoretical concept, the RP may be assessed by Zero-Degree Calorimeters (ZDC) measuring sidewards-kicked spectator neutrons (directed flow v_1). The lower panels of Fig. 3 show AMPT simulation results of $R^{EP}(v_2)$ and $R^{EP}(B_{sq})$, compared to $\pm R_{EP}$ ($R_{EP} \equiv 2(1 - \langle\cos 2(\psi_{EP} - \psi_{RP})\rangle/\mathcal{R}_{EP})/(1 + \langle\cos 2(\psi_{EP} - \psi_{RP})\rangle/\mathcal{R}_{EP})$, where $\mathcal{R}_{EP}$ is the EP resolution).

The commonly used $\Delta\gamma$ variable contains, in addition to the CME it is designed for, v_2-induced background, $\Delta\gamma\{\psi\} = \mathrm{CME}(B_{sq}\{\psi\}) + \mathrm{BKG}(v_2\{\psi\})$. $\Delta\gamma\{\psi\}$ can be measured with respect to $\psi = \psi_{RP}$ (using the 1st order event plane ψ_1 by the ZDC) and $\psi = \psi_{EP}$ (2nd order event plane ψ_2 via final-state particles). If $\mathrm{BKG}(v_2)$ is proportional to v_2 and $\mathrm{CME}(B_{sq})$ to B_{sq} , then

$$R^{\mathrm{EP}}(\Delta\gamma) = 2\frac{r(1 - a^{\mathrm{EP}}_{B_{\mathrm{sq}}}) - (1 - a^{\mathrm{EP}}_{v_2})}{r(1 + a^{\mathrm{EP}}_{B_{\mathrm{sq}}}) + (1 + a^{\mathrm{EP}}_{v_2})} \approx \frac{1 - r}{1 + r} R^{\mathrm{EP}}(v_2)\,. \tag{3}$$

Here $r \equiv \mathrm{CME}(B_{sq}\{\psi_{RP}\})/\mathrm{BKG}(v_2\{\psi_{EP}\})$ can be considered as the relative CME signal to background contribution. If the experimental measurement $R^{EP}(\Delta\gamma)$ equals to $R^{EP}(v_2)$ (i.e. $\Delta\gamma$ scales like v_2), then CME contribution is zero; if $R^{EP}(\Delta\gamma) \approx -R^{EP}(v_2)$ (i.e. $\Delta\gamma$ scales like B_{sq}), then background is close to zero and all would be CME; and if $R(\Delta\gamma) = 0$, then background and CME contributions are of similar magnitudes. Recently, our new method has been applied to experimental data by the STAR collaboration; see Ref. [15] for more details.

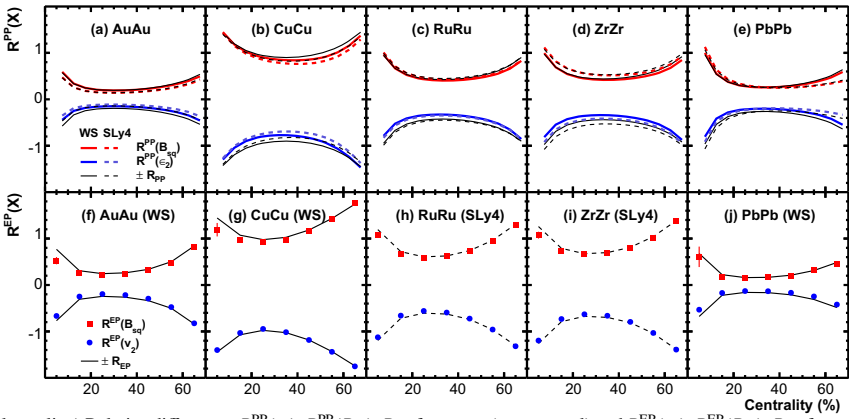

Fig. 3. (Color online) Relative differences $R^{\rm PP}(\epsilon_2)$, $R^{\rm PP}(B_{\rm sq})$, $R_{\rm PP}$ from MCG (upper panel) and $R^{\rm EP}(v_2)$, $R^{\rm EP}(B_{\rm sq})$, $R_{\rm EP}$ from AMPT (lower panel) for (a,f) AuAu, (b,g) CuCu, (c,h) RuRu, and (d,i) ZrZr at RHIC, and (e,j) PbPb at the LHC. Both the WS and DFT-calculated densities are shown for the MCG results, while the used density profiles are noted for the AMPT results. Errors, mostly smaller than the symbol size, are statistical.

4. Summary

To reduce background effects in CME search, isobaric $^{96}_{44}$Ru+$^{96}_{44}$Ru and $^{96}_{40}$Zr+$^{96}_{40}$Zr collisions have been proposed where the v_2-induced backgrounds are expected to be similar while the CME-induced signals to be different. In our study, the proton and neutron density distributions of $^{96}_{44}$Ru and $^{96}_{40}$Zr are calculated using the energy density functional theory (DFT). They are then implemented in the *Monte Carlo* Glauber (MCG) model to calculate the eccentricities (ϵ_2) and magnetic fields (**B**), and in A Multi-Phase Transport (AMPT) model to simulate the v_2. It is found that those nuclear densities, together with the Woods-Saxon (ws) densities, yield wide ranges of differences in $B_{\rm sq}$ with respect to the participant plane (PP) and the reaction plane (RP).

We thus propose a novel method with comparative measurements of $\Delta\gamma$ with respect to $\psi_{\rm RP}$ and $\psi_{\rm PP}$ in the same collision system. Our method is superior to isobaric collisions where large systematics persist. The novel method has been applied to experimental data by the STAR collaboration. With improved statistics, the novel method we report here should be able to decisively answer the question of the CME in quantum chromodynamics.

This work was supported in part by the National Natural Science Foundation of China under Grants No. 11647306, 11747312, U1732138, 11505056, 11605054, and 11628508, and US Department of Energy under Grant No. DE-SC0012910.

References

[1] D. Kharzeev, R. D. Pisarski, M. H. G. Tytgat, Phys. Rev. Lett. 81 (1998) 512–515.
[2] D. E. Kharzeev, J. Liao, S. A. Voloshin and G. Wang, Prog. Part. Nucl. Phys. 88 (2016) 1.
[3] J. Zhao, Int. J. Mod. Phys. A33 (13) (2018) 1830010.
[4] S. A. Voloshin, Phys. Rev. C70 (2004) 057901.
[5] L. Adamczyk, et al. (STAR Collaboration), Phys. Rev. Lett. 113 (2014) 052302; Phys. Rev. C88 (2013) 064911.
[6] F. Wang, Phys. Rev. C81 (2010) 064902; A. Bzdak, V. Koch and J. Liao, Phys. Rev. C83 (2011) 014905; S. Pratt, S. Schlichting and S. Gavin, Phys. Rev. C84 (2011) 024909; F. Wang and J. Zhao, Phys. Rev. C95 (2017) 051901.
[7] S. A. Voloshin, Phys. Rev. Lett. 105 (2010) 172301.
[8] W.-T. Deng, X.-G. Huang, G.-L. Ma, G. Wang, Phys. Rev. C94 (2016) 041901.
[9] H.-j. Xu, X. Wang, H. Li, J. Zhao, Z.-W. Lin, C. Shen, F. Wang, Phys. Rev. Lett. 121 (2018) 022301.
[10] H.-j. Xu, J. Zhao, X. Wang, H. Li, Z.-W. Lin, C. Shen, F. Wang, Chin. Phys. C42 (2018) 084103.
[11] X. B. Wang, J. L. Friar, A. C. Hayes, Phys. Rev. C94 (3) (2016) 034314.
[12] H.-j. Xu, L. Pang, Q. Wang, Phys. Rev. C89 (6) (2014) 064902.
[13] W.-T. Deng, X.-G. Huang, Phys. Rev. C85 (2012) 044907.
[14] Z.-W. Lin, C. M. Ko, B.-A. Li, B. Zhang, S. Pal, Phys. Rev. C72 (2005) 064901.
[15] J. Zhao, Quark Matter 2018 proceedings, arXiv:1807.09925.